Proceedings of the 2006 WSEAS/IASME International Conference on Fluid Mechanics, Miami, Florida, USA, January 18-20, 2006 (pp7-12)

Particle Dynamics in Plane Wake-Type Flows

ZUO-BING WU
State Key Laboratory of Nonlinear Mechanics,
Institute of Mechanics, Chinese Academy of Sciences,
Beijing 100080, CHINA

Abstract: In this paper, particle dynamics in relation to particle size is exploited in two plane wake-type flows. For the motion of particles in the Karman vortex street flow, along with an increase of the particle size, trajectories have a route of period-doubling bifurcation to a chaotic orbit. For the particle motion in a plane wake flow, spectral element method is employed to provide an instantaneous flow field, so that a detail classification of particle patterns in relation to Stokes and Froude numbers is determined. It is found that particle motion feature only depends on Stokes number at a high Froude number and depends on both numbers at a low Froude number. A parameter describing Stokes number divided by Froude number is introduced to make a threshold of the different effects on the particle motion.

Key-Words: Plane wake-type flow, Particle dynamics, Spectral element method

1 Introduction

The motion of particles in a nonuniform flow has wide technological applications, such as to increase combustion efficiency and forecast environmental pollution [1,2]. To understand flow mechanism, some theoretical models and computational methods are developed in the particulate two-phase flow research. Due to particle motion in the low Reynolds number category, the equation of motion for a small rigid sphere in a nonuniform flow field is proposed [3,4]. Related studies show that even when the background flow fields are very simple, the motion can have abundant phenomena: suspended particles accumulate along simple isolated curves for a cellular flow field [5] and periodic, quasiperiodic or chaotic trajectories for a periodic Stuart vortex flow [6].

In both a plane mixing layer and wake flow, influences of large-scale vortices on the particle dispersion process are observed experimentally and simulated by discrete vortex method [7]. In a plane mixing layer, the particles are found to concentrate near the outer edges of the vortex structures. It can be described by the particle sheet stretching and folding mechanisms in vortex pairing interactions [8]. For the particle dispersion in a plane wake flow at a high Reynolds number (10^4), highly organized patterns of particle concentrations are produced in a correlation with the Stokes number. The particles at intermediate Stokes number are focused into sheet-like regions near the boundaries of the large scale vortex structures [9,10].

To analyze numerically interaction of particles with vortices in plane wake-type flows, in this paper, both a Karman vortex street flow and a plane wake flow behind a circular cylinder at a moderate Reynolds number (10^2) are taken as background flows. For the Karman vortex street flow, effects of particle size on trajectories are considered. For the plane wake flow, an instantaneously flow field is obtained in solving Navier-Stokes equations by high-order splitting schemes [11] and spectral element method [12,13], so that a detail classification of the patterns of particles interacting with vortices in relation to Stokes and Froude numbers is determined.

2 Governing Equations

The motion of a small spherical particle in a nonuniform flow field $\mathbf{u}$ is governed by the momentum equation [3,4,6]

$$\frac{\pi}{6} d_p^3(\rho_p + 0.5\rho_f)\frac{d\mathbf{V}}{dt} = \frac{\pi}{6} d_p^3(\rho_p - \rho_f)\mathbf{g} + \frac{\pi}{4} d_p^3 \rho_f \frac{D\mathbf{u}}{Dt} + 3\pi d_p \nu_f \rho_f (\mathbf{u}-\mathbf{V}) f_d + \frac{3}{2}(\pi\nu_f)^{1/2} d_p^2 \rho_f \int_0^t \frac{1}{\sqrt{t-\tau}}\left(\frac{d\mathbf{u}}{dt} - \frac{d\mathbf{V}}{dt}\right)d\tau + \frac{\pi}{12} d_p^3 \rho_f (\mathbf{u}-\mathbf{V})\times\boldsymbol{\varpi}, \quad (1)$$

where $\mathbf{V}$ is the velocity of the particle, d_p is the particle diameter, ρ is the density, $\mathbf{g}$ is the gravitational acceleration, ν_f is the fluid kinematic viscosity, $\boldsymbol{\omega}$ is the vorticity of the flow fluid, and the subscripts f and p refer to the fluid and particle, respectively. The derivatives D/Dt and d/dt are used to denote a time derivative following a fluid element and the moving sphere, respectively. The parameter f_d relating to Reynolds number of particle ($Re_p=|\mathbf{u}-\mathbf{V}|d_p/\nu_f$) is described [14] as

$$f_d = 1 + 0.1315\,\mathrm{Re}_p^{0.82-0.05\log_{10}\mathrm{Re}_p}, \quad 0.01 < \mathrm{Re}_p \le 20. \quad (2)$$

Introducing the dimensionless quantities $\delta=\rho_p/\rho_f$, $\varepsilon=1/(0.5+\delta)$, $\mathbf{x}^*=\mathbf{x}/L$, $t^*=t/(L/U_\infty)$, $\mathbf{u}^*=\mathbf{u}/U_\infty$, $\mathbf{V}^*=\mathbf{V}/U_\infty$ and $\mathbf{g}^*=\mathbf{g}/g$, we nondimensionlize Eq. (1) and describe as follows

$$\frac{d\mathbf{V}}{dt}=\frac{(1-1.5\varepsilon)}{F_r}\mathbf{g}+\frac{3\varepsilon}{2}\frac{D\mathbf{u}}{Dt}+\frac{f_d}{S_t}(\mathbf{u}-\mathbf{V})$$
$$+3\sqrt{\frac{\varepsilon}{2\pi S_t}}\int_0^t\frac{1}{\sqrt{t-\tau}}(\frac{d\mathbf{u}}{d\tau}-\frac{d\mathbf{V}}{d\tau})d\tau+\frac{\varepsilon}{2}(\mathbf{u}-\mathbf{V})\times\varpi, \quad (3)$$

where the Froude number $F_r=U_\infty^2/(gL)$ (U_∞ and L are the free-stream velocity and the characteristic length, respectively), the Stokes number $S_t=U_\infty T/L$ (T is the particle viscous relaxation time $d_p^2/18\varepsilon\nu_f$), and the asterisks "*" for the dimensionless quantities are omitted for convenience. Moreover, Reynolds number of the particle is written as $Re_p=\check{R}e_p|\mathbf{u}\text{-}\mathbf{V}|$ ($\check{R}e_p=U_\infty d_p/\nu_f$).

The incompressible plane wake-type flow field $\mathbf{u}$ is governed by the Navier-Stokes equations in the form

$$\nabla\bullet\mathbf{u}=0,$$
$$\frac{\partial\mathbf{u}}{\partial t}=-\nabla\mathbf{p}+N(\mathbf{u})+\frac{1}{\mathrm{Re}}L(\mathbf{u}), \quad (4)$$
$$N(\mathbf{u})=-\frac{1}{2}[\mathbf{u}\bullet\nabla\mathbf{u}+\nabla\bullet\mathbf{uu}],\ L(\mathbf{u})=\nabla^2\mathbf{u},$$

where $\mathbf{p}$ is the fluid pressure divided by fluid density and $Re=U_\infty L/\nu_f$ is Reynolds number of the flow.

The particle parameters in Eq.(3) can be taken as d_p=O(10^{-6})m - O(10^{-4})m and ρ_p=2.4 x 10^3kg/m^3 from [9]. Since air is chosen as the fluid media in the flow, the properties of fluid in Eq.(3) are described as ρ_f=1.225kg/m^3 and ν_f=1.45 x 10^{-5}m^2/s [15]. The free-stream velocity is taken as U_∞= O(1) m/s. In order to understand the particle dynamics, we analyze orders of magnitude of parameters in Eq.(3). For giving physical values in the calculation, the parameters f_d and F_r appear to be on the order 1 and 10^{-2}. Since the δ is fixed as the order 10^3, the parameter ε appears to be on the order 10^{-3}. When d_p is taken as the order 10^{-6}m - 10^{-4}m, the parameters T and S_t appear to be on the order 10^{-5}s - 10^{-1}s and 10^{-2} - 10^2, respectively. In this case, the stress tensor term of fluid 3ε/2 $D\mathbf{u}/Dt$, the Basset history term $3\sqrt{\frac{\varepsilon}{2\pi S_t}}\int_0^t\frac{1}{\sqrt{t-\tau}}(\frac{d\mathbf{u}}{dt}-\frac{d\mathbf{V}}{d\tau})d\tau$ and lift force term ε/2 (**u**-**V**) x **ω** have smaller orders than the drag term $f_d/S_t(\mathbf{u}\text{-}\mathbf{V})$ and gravity term $(1\text{-}1.5\varepsilon)/F_r\mathbf{g}$ in the Eq.(3). Thus, the Eq.(3) is dominated by the drag term and gravity term. The particle motion is described by a four-dimensional dynamical system of the form

$$\dot{x}=V_x, \quad (5)$$
$$\dot{y}=V_y, \quad (6)$$
$$\dot{V}_x=f_d/S_t\,(u_x-V_x), \quad (7)$$
$$\dot{V}_y=f_d/S_t\,(u_y-V_y)-1-1.5\varepsilon/F_r. \quad (8)$$

3 Results and Discussion

3.1 A Karman vortex street flow

The velocity filed of Karman vortex street flow is governed by

$$u_x=\frac{\Gamma}{2}[\frac{sh2\pi(y-h/2)}{ch2\pi(y-h/2)-\kappa\cos2\pi x}$$
$$-\frac{sh2\pi(y+h/2)}{ch2\pi(y+h/2)+\kappa\cos2\pi x}]+\frac{\Gamma}{2}\frac{sh2\pi h}{ch2\pi h+\kappa}, \quad (9)$$
$$u_y=-\frac{\Gamma\kappa}{2}[\frac{1}{ch2\pi(y-h/2)-\kappa\cos2\pi x}$$
$$+\frac{1}{ch2\pi(y+h/2)+\kappa\cos2\pi x}]\sin2\pi x,$$

where the streamwise spacing of vortices l is taken as the characteristic length and a parameter κ is introduced to remove singularities.

Using a fourth-order Runge-Kutta algorithm, we integrate Eqs. (5)-(8) with a time size $\Delta t=0.01LT/U_\infty$. The parameters of flow field in Eq. (9) are taken as Γ=1, h=0.3 and κ=0.99. In order to draw a bifurcation diagram and particle trajectories, 20 x 100 points in the street with their corresponding flow filed velocities are taken as initial conditions of Eqs. (5)-(8), respectively. We investigate the motion of particles under the variation of d_p for l=0.1m. In the total 21000 time steps, points in the first 20000 time steps are discarded as transients, as well as points in the following 1000 time steps are plotted as particle trajectories. In the particle trajectories, points y at x=0 versus d_p are plotted as a bifurcation diagram. For a dense bifurcation zone, the diagram is calculated

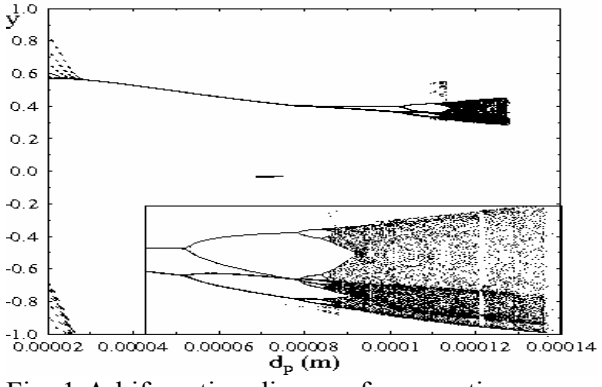

Fig. 1 A bifurcation diagram for a continuous range of d_p showing the vertical position of particles at x=0. The dense bifurcation zone is enlarged and redrawn in the bottom-right corner of the figure.

again by using a smaller time size Δt=0.001LT/U_∞ and enlarged.

In order to display the influence of particle size on the particle motion, we plot a bifurcation diagram $y \sim d_p$ in Fig.1. When d_p<2.62 x 10^{-5}m, the velocity of particle motion is very slow, so that most of the particle trajectories are kept near the vortex street, as well as divided into two sets: one above the vortex street, the other under the vortex street. When $d_p \geq$2.62 x 10^{-5}m, particle trajectories under the vortex street leave farther from the vortex street, but the particle trajectories above the vortex street converge on a period-1 orbit. For d_p=2.62 x 10^{-5}m - 7.85 x 10^{-5}m, period-1 orbits above the vortex street are presented as particle trajectories. Specially, for d_p=6.87 x 10^{-5}m - 7.48 x 10^{-5}m, another period-1 orbit appears in the vortex street. In this case, there exist two attractors for the particle trajectories. As d_p=7.85 x 10^{-5}m, the period-1 orbit bifurcates to a period-2 orbit. For d_p=7.85 x 10^{-5}m - 1.03 x 10^{-4}m, particle trajectories are presented as period-2 orbits. As d_p=1.03 x 10^{-4}m, the period-2 orbit bifurcates to a period-4 orbit. For d_p=1.03 x 10^{-4}m - 1.10 x 10^{-4}m, particle trajectories converge on period-4 orbits. When d_p >1.10 x 10^{-4}m, the period-4 orbit bifurcates further to a period-8 orbit and finally to a quasi-periodic or chaotic orbit. This bifurcation behavior is clearly presented in the enlarged zone in Fig.1. At d_p =1.276 x 10^{-4}m, a crisis happens, so that the quasi-periodic or chaotic orbit disappears, i.e., escapes from the central region of flow. Moreover, a similar bifurcation process emerges in a range near d_p =1.1 x 10^{-4}m.

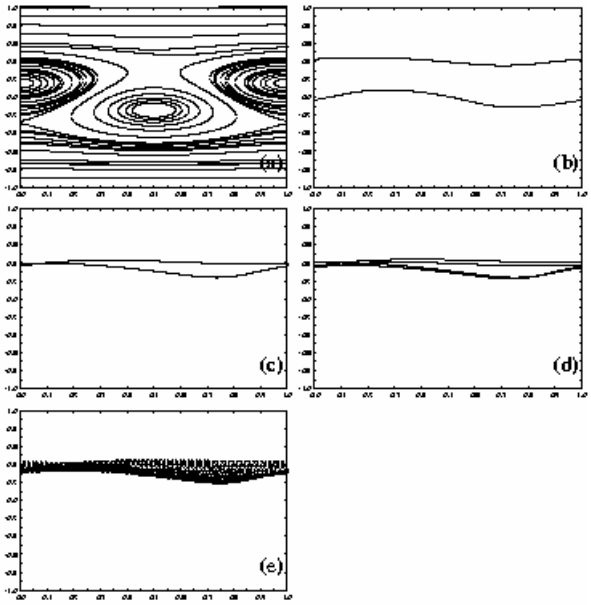

Fig. 2 Typical trajectories on the x-y plane for (a) d_p=3 x 10^{-5} m and all streamlines; (b) d_p=7 x 10^{-5}m; (c) d_p=1 x 10^{-4}m; (d) d_p=1.05 x 10^{-4}m; (e) d_p=1.2 x 10^{-4}m.

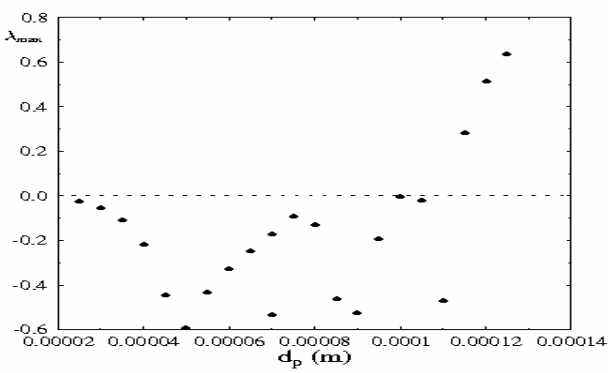

Fig. 3 Variation of the maximal Lyapunov exponent λ_{max} with d_p.

In the following, we give some trajectories for different values of d_p. Concerning the stability of orbits, we take x=0 as a Poincare section and determine their maximal Lyapunov exponents. In Fig.2(a), for d_p=3 x 10^{-5}m, a period-1 orbit and all corresponding streamlines are drawn. The period-1 orbit, where the particles move from left to right, distributes above the vortex street. In Fig.3, for the period-1 orbit, the maximal Lyapunov exponent is -0.05, so the orbit is stable. In Fig.2(b), for d_p=7 x 10^{-5}m, two period-1 orbits are placed above and in the vortex street, respectively. On the orbit above the vortex street, the particles move from left to right. In Fig.3, the maximal Lyapunov exponent of the period-1 orbit is -0.17, so the orbit is stable. But, on the orbit in the vortex street, the particles move in an opposite direction, i. e., from right to left. The maximal Lyapunov exponent of the period-1 orbit is -0.53, so the orbit is also stable. In Fig.2(c), for d_p=1 x 10^{-4}m, a period-2 orbit, which distributes above the vortex street, is drawn as particle trajectories. On the orbit, the particles move from left to right. In Fig.3, the maximal Lyapunov exponent of the period-2 orbit is -0.003, so the orbit is stable. In Fig.2(d), for d_p=1.05 x 10^{-4}m, a period-4 orbit is drawn above the vortex street. On the orbit, the particles move from left to right. In Fig.3, the maximal Lyapunov exponent of the period-4 orbit is -0.02, so the orbit is stable. In Fig.2(e), for d_p=1.2 x 10^{-4}m, a quasi-periodic or chaotic orbit is drawn above the vortex street. On the orbit, the particles move from left to right. In Fig.3, the maximal Lyapunov exponent of the orbit is 0.51, so the orbit is chaotic.

From above results, we can conclude that due to the interaction of particles with vortices in the Karman vortex street flow, along with the increase of particle size, the particle trajectories bifurcate from periodic orbits to chaotic orbits.

3.2 A plane wake flow behind a circular cylinder

The plane wake flow field $\mathbf{u}(\mathbf{x}^n, t^n)$ is obtained by solving Navier-Stokes equations (4). The

time-discretization of the Navier-Stokes equations employs a high-order splitting algorithm. The semi-discrete formulation is written as

$$\frac{\bar{\mathbf{u}}-\sum_{q=0}^{J-1}\alpha_q \mathbf{u}^{n-q}}{\Delta t}=\sum_{q=0}^{J-1}\beta_q N(\mathbf{u}^{n-q}),$$
$$\frac{\bar{\bar{\mathbf{u}}}-\bar{\mathbf{u}}}{\Delta t}=-\nabla p^{n+1}, \nabla\bullet\bar{\bar{\mathbf{u}}}=0, \qquad (10)$$
$$\frac{\gamma_0\mathbf{u}^{n+1}-\bar{\bar{\mathbf{u}}}}{\Delta t}=\frac{1}{\mathrm{Re}}\nabla^2\mathbf{u}^{n+1},$$

where the diameter of circular cylinder is taken as the characteristic length. $\bar{\mathbf{u}}$, $\bar{\bar{\mathbf{u}}}$ are intermediate velocity fields and the constants α_q, β_q and γ_0 are integration coefficients for a mixed explicit/implicit stiffly-stable scheme of order J=3. The spatial discretization of Eq. (10) is obtained by using the spectral element method. The spatial discretization proceeds by first covering the computational domain with general quadrangles. Each quadrangle is mapped from the physical space (x, y) into the local co-ordinate system (r, s) by an isoparametric tensor-product mapping

$$(x,y)_N^k=\sum_{i=0}^{N}\sum_{j=0}^{N}(X,Y)_{ij}^k h_i(r)h_j(s), \qquad (11)$$

where $h_i(r)$ are Nth order local Lagrange interpolants and defined as $h_i(r_j)=\delta_{ij}$. δ_{ij} is the Kronecker-delta symbol. In each isoparametric element, the velocity and pressure are interpolated in the same fashion.

In the calculation parameters used are: the element number is 116, the order of interpolation function is N=8, the streamwise length is 38, and the transverse wide is 11. A spectral element mesh is drawn in Fig.4. Boundary conditions required for the velocity and pressure fields are: at the surface of the cylinder the fluid velocity satisfies the non-slip condition: $\mathbf{u}$=(0,0). Far away from the cylinder and outside the wake, it matches the free-stream velocity $\mathbf{u}$=(1,0) along the left boundary and $\partial u_x/\partial n$ =0, u_y =0 along the up and down boundaries. Across the outflow plane downstream the approximate boundary condition for the velocity field is $\partial_x\mathbf{u}(\mathbf{x},t)$=(0,0). At the same location the pressure is set to a constant value of zero. Along all other boundaries the pressure satisfies the high-order Neumann boundary condition. The time size Δt is taken as 0.002.

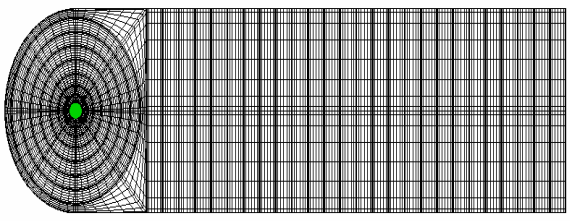

Fig. 4 A spectral element mesh with 8th order local Lagrange interpolants.

From three points near the circular cylinder, particle injection rates in the x direction are kept at a low value of 0.01m/s, which may reduce the coupling effects on the wake flow from the presence of the particles. Using a fourth-order Runge-Kutta algorithm, we integrate Eqs. (5)-(8) with a time size $\tau=2\Delta t$. At each time step 20τ, a particle is injected into the flow field. In order to avoid complex treatment for the interaction between particles and the circular cylinder, we take a numerical boundary r_0=0.6 for the particles. When a particle moves into the boundary, a repelling potential $1/r$ will be added to the particle. At the same time, in order to reduce effects of repelling potential on particle inertia, absolute values of velocity are fixed as 0.01 in the numerical boundary region. For some parameters of particles, Δt and r_0 will decreases and increases, respectively, so that particles can be always separated from the circular cylinder.

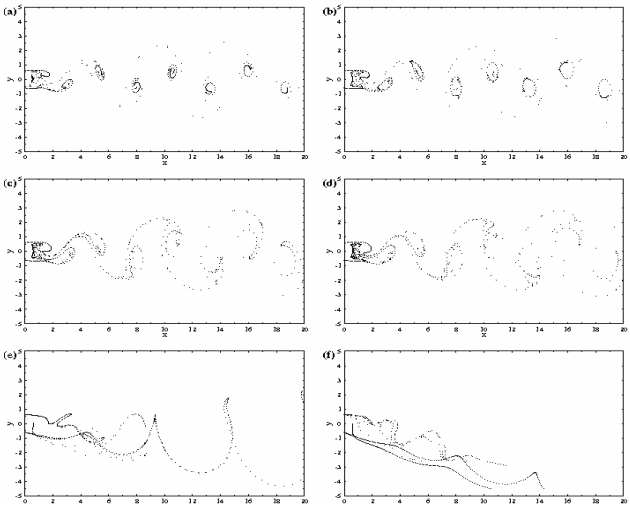

Fig. 5 Particle trajectory patterns in the plane wake flow at different particle size (Stokes number) and a fixed F_r=70.3. (a) d_p=1 x 10^{-6}m (S_t=5.2 x 10^{-2}); (b) d_p = 5 x 10^{-6}m (S_t=0.13); (c) d_p = 8 x 10-6m (S_t=0.33); (d) d_p = 1.5 x 10^{-5}m (S_t=1.2); (e) d_p = 4 x 10^{-5}m (S_t=8.3); (f) d_p = 7 x 10^{-5}m (S_t=18.6).

In Eqs. (7)-(8), S_t affects the particle motions in both x and y directions. However, F_r can only make changes of particle motion in the y direction. A different combination of S_t and F_r determine the particle motion in the plane wake flow. For a given Re, the Stokes and Froude numbers can be deduced as $S_t=U_\infty^2 d_p^2/18\varepsilon v_f^2 Re$ and $F_r= U_\infty^3/g v_f Re$. Firstly, we investigate effects of S_t on the particle motion at a fixed F_r. Since U_∞ is taken as 1m/s, F_r is fixed at 70.3. Along with the increase of particle size or Stokes number, organized structures of particles in the interaction with the Karman vortex street are evaluated. Some basic features of particle trajectories are drawn in Fig. 5. The particles follow the Karman vortex street to downstream and interact with the

vortices. In a range of d_p=1 x 10^{-6}m to 3 x 10^{-6}m (S_t=5.2 x 10^{-3} to 4.7 x 10^{-2}), the particles mainly fill the cores of vortices as drown in Fig. 5(a). In a range of d_p=5 x 10^{-6}m to 8 x 10^{-6}m (S_t=0.13 to 0.33), the particles move from the cores of vortices to outside of the cores as drawn in Fig. 5(b)-(c). In a range of d_p=1 x 10^{-5}m to 2 x 10^{-5}m (S_t=0.52 to 2.1), the particles concentrate at the edge of vortex street as drawn in Fig. 5(d). In a range of d_p=3 x 10^{-5}m to 4 x 10^{-5}m (S_t=4.7 to 8.3), the particles, which concentrate at the edge of vortex street, have a main distribution in the down region as drawn in Fig. 5(e). In a range of d_p=5 x 10^{-5}m to 7 x 10^{-5}m (S_t=12.9 to 24.3), the particles escape from the central region of vortex street as drawn in Fig. 5(f). Thus, at a fixed F_r, along with the increase of S_t, the particle motion feature evaluates from a centralized distribution to a global distribution in the central region of the vortex street. The solid particles company the vortices to move downstream and have larger transverse velocities than the fluid particles in the increase of S_t. In final, the transverse velocities of particles are large enough, so that they escape from the central region of the vortex street.

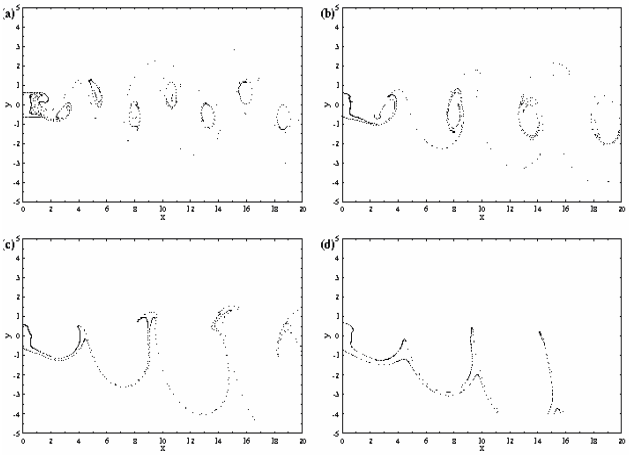

Fig. 6 Particle trajectory patterns in the plane wake flow at different Froude and a fixed S_t=0.13. (a) F_r=70.3 (κ=1.8 x 10^{-3}); (b) F_r = 1.1 (κ=0.12); (c) F_r = 0.56 (κ=0.23); (d) F_r = 0.41 (κ=0.32).

Secondly, we investigate effects of F_r on the particle motion at a fixed S_t. Since F_r only depends on U_∞, to preserve a fixed S_t, d_p will be changed in the fluctuation of U_∞. For the fixed S_t=0.13, we take some different F_r to display phenomena of particle motion. When F_r = 4.5 x 10^3, 5.6 x 10^2, 70.3, and 8.8, the moved particles preserve at the cores of vortices as drawn in Fig. 6(a), which is the similar to the phenomenon described in Fig. 5(a). However, when F_r= 1.1 in Fig. 6(b) and 0.56 in Fig. 6(c), the particle motion has different phenomena described in Fig. 5(a). Many particles move from the up level vortices in the vortex street to the down level ones. At the same time, the particles move from the cores of vortices to outside of the cores and the edge of the vortex street. When F_r = 0.24 and 0.14, all particles concentrate in the down level vortices in the vortex street and the down edge of vortex street as drawn in Fig. 6(d). Along with the increase of streamwise distance, the particles escape from the central region of the vortex street. We also investigate the particle motion feature at fixed S_t=4.7 x 10^{-2} and 2.1, the global phenomena are similar to those described as above, but have different thresholds for the effects of F_r.

In order to display the effects of F_r on the particle motion, we introduce a parameter $\kappa = F_r^{-1}/S_t^{-1}=S_t/F_r$. When $\kappa \leq 0.05$, the patterns of particle motion only depend on S_t and distribute in the central region of vortex street. The Stokes drag term is a major term in Eqs. (7)-(8). The gravity term can be neglected. When $0.05<\kappa\leq 0.25$, the moved particles concentrate the down region of vortex street and has only a few of particles in the up region of vortex street. The gravity term is a major term in Eq. (8), but the Stokes term cannot be neglected. When $0.25<\kappa$, the particles escape from the central region of vortex street along with the increase of streamwise distance. The Stokes term in Eq. (8) can be neglected. Since the particle motion feature evaluates continuously along with a continuous change of F_r, the thresholds 0.05 and 0.25 are only approximate ones. However, they can still provide a qualitative criterion for the effects of F_r.

4 Conclusion

In summary, we have shown that in two plane wake-type flows, particle size influences on particle motion trajectories. Due to the interaction of particles with vortices in a Karman vortex street flow, along with increase of the particle size, a period-doubling bifurcation to a chaotic orbit emerges. For the particle motion in a plane wake flow at a moderate Reynolds number, an instantaneous flow field is obtained by using the spectral element method, so that a detail classification of the patterns in relation to Stokes and Froude numbers is determined. It is found that particle motion feature only depends on Stokes number at a high Froude number and depends on both numbers at a low Froude number. A parameter κ describing Stokes number divided by Froude number is proposed to make a threshold of the different effects on the particle motion. When $\kappa \leq 0.05$, the patterns of particle motion only depend on Stokes number and distribute in the central region of the vortex street. When $0.05<\kappa\leq 0.25$, the moved particles concentrate the down region of vortex street and has only a few of particles in the up region of

vortex street. When $0.25<\kappa$, the particles escape from the central region of vortex street along with the increase of streamwise distance.

Acknowledgments: This work was supported in part by the National Key Program G1999032801 and the CAS Program KJCX2-SW-L2 and the K. C. Wong Education Foundation of Hong Kong. We also thank LSEC and ICTS research computing facilities for assisting us in the computation.

References:

[1] J. C. Hunt, Industrial and environmental fluid mechanics, *Ann. Rev. Fluid Mech.* Vol. 23, 1991, pp.1-42.

[2] C. T. Crowe, J. N. Chung and T. R. Troutt, Particle dispersion by organized turbulent structures, in *Particulate Two-Phase Flow*, ed. M. C. Roco, Butterworth-Heinemann, London, 1993, pp. 626-669.

[3] M. R. Maxey and J. J. Riley, Equation of motion for a small rigid sphere in a nonuniform flow, *Phys. Fluids* Vol. 26, 1983, pp. 883-889.

[4] T. R. Auton, J. C. R. Hunt and M. Prud'homm, The force exerted on a body in an inviscid unsteady non-uniform rotation flow, *J. Fluid Mech.* Vol.197, 1988, pp. 241-257.

[5] M. R. Maxey, The motion of small spherical particles in a cellular flow field, *Phys. Fluids* Vol. 30, 1987, pp. 1915-1928.

[6] K.-K. Tio, A. M. Ganan-Calvo and J. C. Lasheras, The dynamics of small, heavy, rigid spherical particles in a periodic Stuart vortex flow, *Phys. Fluids A* Vol. 5, 1993, pp. 1679-1693.

[7] C. T. Crowe, J. N. Chung and T. R. Troutt, Particle interaction with vortices, in *Fluid Vortices*, ed. S. I. Green, Kluwer Academic Publishers, Dordrecht, 1995, pp. 829-861.

[8] F. Wen, N. Kamalu, J. N. Chung, C. T. Crowe and T. R. Troutt, Particle dispersion by vortex structures in plane mixing layers, *J. Fluids Eng.* Vol. 114, 1992, pp. 657-666.

[9] L. Tang, F. Wen, Y. Yang, C. T. Crowe, J. N. Chung and T. R. Troutt, Self-organizing particle dispersion mechanism in a plane wake, *Phys. Fluids A* Vol. 4, 1992, pp. 2244-2251.

[10] Y. Yang, C. T. Crowe, J. N. Chung and T. R. Troutt, Experiments on particle dispersion in a plane wake, *Inter. J. Multiphase Flow* Vol. 26, 2000, pp. 1583-1607.

[11] G. E. Karniadakis, M. Israeli and S. A. Orszag, High-order splitting methods for the incompressible Navier-Stokes equations, *J. Comput. Phys.* Vol. 97, 1991, pp. 414-443.

[12] A. T. Patera, A spectral element method for fluid dynamics: laminar flow in a channel expansion, *J. Comput. Phys.* Vol. 54, 1984, pp. 468-488.

[13] K. Z. Korczak and A. T. Patera, An isoparametric spectral element method for solution of the Navier-Stokes equations in complex geometry, *J. Comput. Phys.* Vol. 62, 1986, pp. 361-382.

[14] R. Clift, J. R. Grace and M. E. Weber, *Bubbles, Drops and Particles*, Academic, New York, 1978.

[15] R. L. Panton, *Incompressible Flow*, John Wiley & Sons, New York, 1984.